Load-Balancing Multi-LCD Light Field Display

Xuan Cao*, Zheng Geng, Mei Zhang, Xiao Zhang
State Key Laboratory of Management and Control for Complex Systems, Institute of Automation, Chinese Academy of Sciences, Beijing, 100190, China

ABSTRACT

We propose a load-balancing multi-LCD light field display technology. The multiple LCD panels operate as a spatial light modulator. Each light ray is the combination of pixels located in multiple LCD panels. The challenging problem is how to decompose the light field into limited layer images and display the light field compressively. Each pixel, as a controllable unit, is in spatial-multiplexing which means one pixel needs to be responsible to modulate multiple target light rays at the same time. We analyze the load imposed on each pixel by casting the light field decomposition as an over-determined equation problem. We found each pixel works in the state of overload and single pixel couldn't give consideration to all target light rays. In order to reduce the load on pixels and improve display fidelity, we develop a multi-layer and multi-zone joint optimization strategy. The target light field is divided into multiple subzones and each subzone is displayed by multiple LCD panels combining with a dynamic directional backlight. By resolving the target light field, our display system further explores the multi-LCD's capability of displaying light field and higher quality of light field display is achieved. We test our load-balancing decomposition algorithm based on different scene. The parallax, occlusion and blur of out-of-focus are restored successfully. And a three-layer prototype is constructed to demonstrate that correct light field is displayed in indoor lighting environment.

Keywords: light field display, multi-LCD, light field decomposition, joint optimization, nonnegative tensor factorization, dynamic directional backlight

1. INTRODUCTION

1.1 Autostereoscopic display

Autostereoscopic display aroused researchers' interest all over the world, providing richer perceptual depth cues than traditional 2D display and removing the eyewear. Following the classification in [Lipton et al. 1982][1], depth cues contains two main categories: 1) Monocular cues can be perceived by signal eye, including perspective, shading, motion parallax, occlusion and accommodation. 2) Binocular cues need cooperation of two eyes, containing disparity and convergence. Traditional 2D display provides limited depth cues, mainly belonged to psychological cues, including perspective, shading and occlusion. Autostereoscopic display extends human's visual perception more or less by different technologies.

Generally, autostereoscopic display mainly contains volumetric displays, holograms, parallax barriers and integral imaging[2]. The recent volumetric displays[3,4], providing 360 degree light field, inevitably need mechanical motion which resulting in complicated synchronous control system and cumbersome hardware assembling. Hologram, providing almost all depth cues, is currently on the stage of displaying static scenes. Parallax barriers and integral imaging have been adopted by some manufactures to product consumer-grade glass-free display devices at price of decreased resolution. In addition, the barrier adopted in commercial products is static which restricts viewers to get good 3D visual experience only in discrete and limited viewpoints. Along with the development of light field photograph[5,6,7], light field source is not the primary hinder to autostereoscopic technologies. An effective, depth cues-rich and low-cost display technology becomes in demand.

1.2 Multiple LCDs stack

Recently, stack of liquid crystal display (LCD) panels[8,9] provides off-the-shelf solution for 3D display, which can be operated as dynamic parallax barrier. This compressive display technology exhibits more superiority than previous schemes, including mechanical movement-free, low-cost, higher brightness. [Wetzstein et al. 2011][10] further represented light field with tensor and developed a multilayer-multiframe joint optimization framework. The display fidelity depended

Stereoscopic Displays and Applications XXVI, edited by Nicolas S. Holliman, Andrew J. Woods, Gregg E. Favalora, Takashi Kawai, Proc. of SPIE-IS&T Electronic Imaging, Vol. 9391, 93910F
 · doi: 10.1117/12.2078366

on LCD layers and was not satisfying by limited number of layers. Increased LCD layers improved display quality slightly but reduced transparency seriously. In this paper, we address similar issues in a novel framework, including analysis of light field decomposition and load-balancing optimization. We analyze light field decomposition in a simple and effective way by casting the problem as a large over-determined equation set rather than complicated tensor factorization. In our scheme, the pixels in multiple LCD are controllable units and the target light rays are assumed as load imposed on such controllable units. We found overload on pixels is the main restriction on improving display quality. Multiple frames bring more degree of freedom[10] but fail to reduce the load in single frame decomposition. We balance the decomposition load by dividing the target light field into multiple subzones and develop a novel multi-layer and multi-zone joint optimization strategy. For displaying each light field zone in sequence, we construct a dynamic directional backlight operated synchronously with multiple LCDs. Considering the loss of display brightness resulted from adding LCD layers, we use LCD layers as less as possible which provides brighter view and more comfortable visual perception.

1.3 Main Contribution

1) Analyzing the load imposed on LCD pixels during light field decomposition by constructing a large over-determined equation set.
2) A novel multi-layer and multi-zone joint optimization and decomposition architecture for Multi-LCD display: reducing the decomposition load and achieving higher light field display quality without adding extra LCDs; less LCD layers increase display brightness and provide better visual perception; the spatial independence and parallelity are future explored.
3) A dynamic directional backlight: combining one LCD panel and lenticular lens but no requirement on slanting lenses; increasing the brightness of backlight by allowing multiple pixels under each lens to illuminate; establishing an independent angle coordinate system for each cylindrical lens and the direction of backlight can be changed flexibly and dynamically; construct a LED array as backlight source to increase display brightness.

2. RELATED WORK

Multiple Layer Display (MLD) is not a novel architecture and the tomographic medium varies widely. [Barnum et al. 2010] displayed voxels on water curtain in different spatial depth by controlling projector and water manifolds synchronously[11]. Researchers found liquid crystal panel is a better tomographic medium due to its transparency and pixel-wise controllability[12,13]. Gotoda also demonstrated multiple layers display has wider depth than flat display[14]. Stack of LCD panels, as an electrically movable pixel barrier[15], increased the image resolution and viewing-angle. Recently, Wetzstein and Lanman did a series of significant works on multi-LCD displays[8,9,10]. Content-adaptive parallax barriers modified the dual-layer LCDs to increase optical efficiency[8]. [Lanman et al. 2011] operated each pixel in multiple LCDs as a polarization rotator to increase the light transmittance[16].

Most previous multi-LCD display technologies trended to operate the viewer-near LCD panel as digital barrier. By representing light field with a tensor, [Wetzstein et al. 2012] further developed a novel optimization framework[10] allowing multi-layer and multi-frame joint optimization. Then the high dimensional light field was decomposed into multiple layers based on nonnegative tensor factorization (NTF)[17,18]. But respectable number of LCD layers and frames were needed to achieve satisfying light field display quality, which seriously reduce the display brightness due to the lower light transmittance of LCD panel. By constructing a large over-determined equation set, we analyze the load level of light field decomposition and found the display fidelity can be improved by alleviating the load level. Inspired by Wetzstein's tensor display, we propose a novel load-balancing light field display architecture which further explores the display capability of multi-LCDs.

3. MULTI-LCD DISPLAY

Before introducing our light field decomposition scheme, we describe parameterization of multiple layers and how to emit a target light field. Multiple LCD layers naturally construct a spatial light modulator which attenuates the light rays emitted from the backlight. The light rays emitted from the backlight panel get through multiple LCD panels and then reach into human's eyes. According to the 4D light field definition[19], one light ray is represented by two points intersected with two parallel planes provided that the light ray is not parallel to the planes. For convenient reference, we define N LCD layers at resolution of $w*h$ as $P(w,h,N)$ and all LCD layers are assumed to have same resolution. Target light field with $v_x * v_y$ views which at resolution of $r_x * r_y$ is defined as $L(v_x, v_y, r_x, r_y)$. The LCD layers N is required not less than 2 (N is 3 in following analysis). The light rays originated from any pixel in one LCD can reach to any pixel in the adjacent LCD. Thus, theoretically, two LCD layers can produce $(w*h)^2$ light rays. It should be noted that the number of light rays produced by more than two LCD layers is also up to $(w*h)^2$. Because one light ray can be restricted by two points and other points in this line is redundant.

As shown in Figure 1, each view in the target light field is produced by the combination of all LCD layers. Each light rays can be traced back to the LCD layers and find the intersection points with each LCD panel, as shown in Figure 2. Considering the physical spatial relative position between the LCD panels and the target light field, as shown in Figure 2, the size of target light filed is generally smaller than the size of LCD. So some marginal pixels in the LCD near to viewers are not activated. All pixels in the LCD farthest to viewer are utilized, so the each view in the target light field has same resolution with LCD.

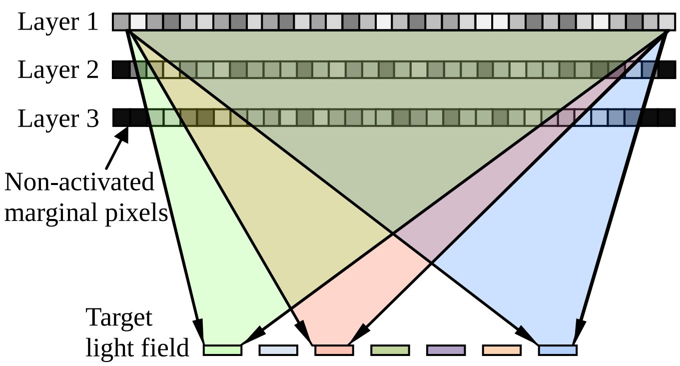

Figure 1. Target light field: each view is produced by all LCD layers

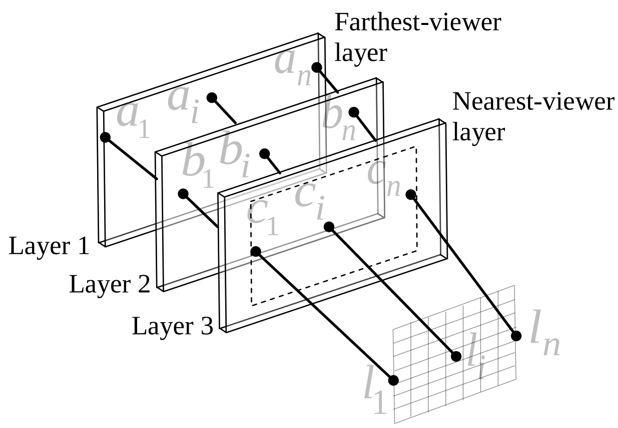

Figure 2. Target rays tracing back to multi-LCD

According to [Wetzstein et al. 2012][10], each target light ray is simply represented by the production of three pixel units:

$$l_i = a_i \times b_i \times c_i$$

We can also express the target light ray by summation of three pixel units in logarithmic field:

$$\log(l_i) = \log(a_i \times b_i \times c_i) = \log(a_i) + \log(b_i) + \log(c_i)$$

where l_i is the target light ray; a_i, b_i and c_i denote the intersection pixels on the three LCD panels along the l_i.

4. LIGHT FIELD DECOMPOSITION SOLVER

An effective solver for the light field decomposition is significant to implement light field display. The direct way to solve the large over-determined equation set is based on pseudo-inverse, which takes very huge computation cost. Simultaneous Algebraic Reconstruction Technique (SART)[20,21] provides an update rule at pixel level but seems not physically meaningful to light field decomposition. Non-negative tensor factorization[17,18] provides a physically meaningful solver to the problem of high-dimensional light field decomposition. Tensor factorization, however, involves massive operation of sparse matrix. We found the computation time can be further reduced by focusing on only solving the non-zero light rays. In a related work, [Wetzstein et al. 2012][10] implemented GPU-based NTF solver by OpenGL and Cg displaying geometry model (e.g. teapot) interactively. But it's not image-based light field decomposition.

In this section, we develop a pixel-level iterative algorithm to update LCD pixels. Only the valid target light rays (non-zero terms in transform matrix as shown in Figure 4) are decomposed to three layers. Our iterative algorithm updates one layer at one time and the rest layers keep fixed before finishing the current layer update. As shown in Figure 3, the pixel a is responsible to emit multiple light rays. And the optimization purpose is to find a "best" value for pixel a forcing all light rays passed through pixel a to be close to the target light rays. As expressed in Eq. (1), our algorithm minimizes the Euclidean distance between a target light field and that emitted by multi-LCD.

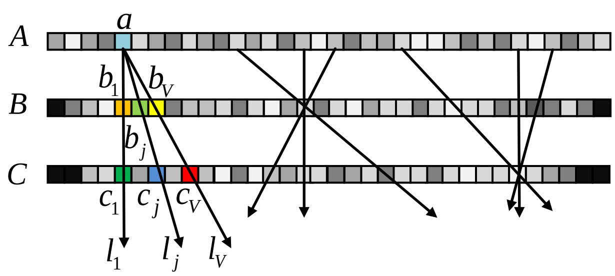

Figure 3. Analysis for load on each pixel in different LCD layer

$$\begin{cases} \min\limits_{a} \quad f(a) = \sum_{j=1}^{V} (L_j - a * b_j * c_j)^2 \\ s.t. \quad 0 \le a \le 1 \end{cases} \tag{1}$$

By forcing the derivative to be zero, we can deduce the update rule for layer A.

$$\begin{cases} \dfrac{df(a)}{da} = \sum_{j=1}^{V} 2(L_j - a * b_j * c_j) * (b_j * c_j) = 0 \\ s.t. \quad 0 \le a \le 1 \end{cases} \tag{2}$$

$$\Rightarrow \begin{cases} a' = \dfrac{\sum_{j=1}^{V} L_j * (b_j * c_j)}{\sum_{j=1}^{V} (b_j * c_j)^2} = a * \dfrac{\sum_{j=1}^{V} L_j * (b_j * c_j)}{\sum_{j=1}^{V} \hat{L}_j * (b_j * c_j)} \\ s.t. \quad 0 \le a' \le 1 \end{cases} \tag{3}$$

where L_j is j-th target light ray passed through pixel a; b_j and c_j is the intersection pixel in layer B and C along with j-th target light ray; V is amount of views in target light field ($V = v_x * v_y$); $\hat{L}_j$ is the j-th reconstructed light ray ($\hat{L}_j = a * b_j * c_j$); a is the old pixel value, and the updated pixel value is denoted as a'.

Following the same deduction method, we figure out the update rules for all three layers, as expressed in Eq. (4). The initial value of LCD pixels is set randomly from 0 to 1 and the pixel value is restricted from 0 to 1. Different initial values may make different results. How to set the initial values remains a promising research direction.

$$\begin{cases} a' = a * \dfrac{\sum_{j=1}^{V} L_j * b_j * c_j}{\sum_{j=1}^{V} \hat{L}_j * b_j * c_j}, \ 0 \le a' \le 1 \\ b' = b * \dfrac{\sum_{j=1}^{V} L_j * a_j * c_j}{\sum_{j=1}^{V} \hat{L}_j * a_j * c_j}, \ 0 \le b' \le 1 \\ c' = c * \dfrac{\sum_{j=1}^{V} L_j * a_j * b_j}{\sum_{j=1}^{V} \hat{L}_j * a_j * b_j}, \ 0 \le c' \le 1 \end{cases} \tag{4}$$

Considering the physical LCD panel, the pixel value must be non-negative. There is no subtraction operation in our iteration algorithm as shown in Eq. (4), so the pixel value keeps non-negative provided that the initial value in first iteration is non-negative. Our iteration algorithm updates the pixel value by multiplication acquiring faster convergence. However the updated pixel value maybe exceeds 1 if the denominator is much less than numerator especially when denominator is zero. We also restrict the pixel value to be less than 1 at end of each iteration to prevent the deviation from being accumulated and expanded.

5. LOAD ANALYSIS OF LIGHT FIELD DECOMPOSITION

As shown in Figure 1, multi-LCD display requires multiple LCD layers to reproduce the target light field compressively. Light field decomposition primarily aims to generate the 2D layer images for compressive display effectively. This section analyzes the light field decomposition from perspective of load balancing.

Every view is displayed by all LCD layers but by different combination of LCD pixels. In other words, each pixel is responsible to produce multiple light rays, as shown in Figure 3. Tensor display[10] constructs a physically meaningful model to represent the high-dimensional light field and decompose light field based on non-negative tensor factorization. But such a complicated model is not good at analyzing the performance of decomposition. We found the light field decomposition can be analyzed in a simple and direct way by casting the decomposition as a problem of solving an over-determined equation set. The target light field and LCD layers are vectorized in same way. In our analysis, we rearrange elements from left to right and row by row. Then the target light rays and the LCD pixels are connected by a transform matrix, as shown in Figure 4.

By projecting the target light rays back to the LCD layers, as shown in Figure 2, the intersection point determines the value of the terms in the transform matrix. Each view is projected back to all LCD layers (7*7 views and 3 LCD layers in this case), and the correspondence between single view and three layers is presented by a sub-matrix, as the chromatic sub-matrix shown in Figure 4. The terms corresponding to intersection points are set as 1 and the rest terms in the transform matrix are zeros. So the transform matrix is sparse and the non-zero terms mainly distribute in diagonals of sub-matrixes. Due to the relative spatial position between each view and the LCD panels is different, every sub-matrix is different. As mentioned in section 3, some marginal pixels in the near-viewer LCD is not be used. Correspondingly, some columns in the transform matrix are full-zero. There is no full-zero row in the transform matrix and there is fixedly three non-zero terms in any signal row. Because every target light ray must be combination of three pixel units.

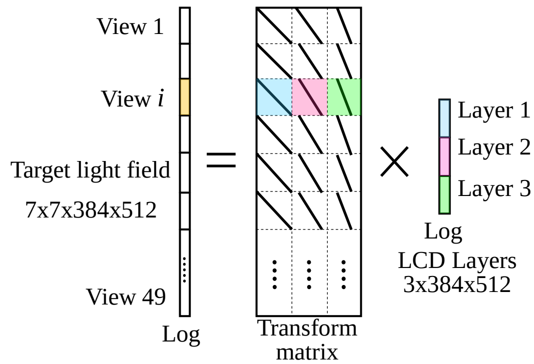

Figure 4. Visualization of transform matrix

Compared to the high dimensional tensor representation[10], the over-determined equation set visualizes the light field decomposition in two dimensions. We assume the target light field as to-be-resolved load. And the pixels in multi-LCD layers are casted as controllable units for producing the target light field. In theory, the upper bound of light rays that can be produced by multiple layers is up to $(w*h)^2$ as mentioned in section 3. Although the total number of target light rays ($v_x * v_y * r_x * r_y$) is much less than the upper bound, controllable units in multi-LCD is too limited to represent the huge number of light rays in target light field. As shown in Figure 3, single pixel in any LCD layer is responsible to produce multiple light rays. More light rays imposed on single pixel means heaver load on the pixel. To some extent, the ratio of amount of light rays to the number of controllable units reflects the average load level. We define the ratio of number of non-zero rows to number of non-zero columns of the transform matrix as load level of light field decomposition. For simplicity, the zero columns (the non-active marginal pixels) are assumed to be negligible. The quantization of load level is expressed in Eq. (5).

$$Load = \frac{Rows_T}{Columns_T} = \frac{v_x * v_y * r_x * r_y}{w * h * N} \tag{5}$$

Larger load level means single pixel unit need to take responsibility for more target light rays. When load level is 1, one pixel is in charge for one light ray and the target light field can be displayed without fidelity loss. On the contrary, some pixel units are wasted if load level is less than 1. Considering three LCD layers and a 7*7 light field in same resolution with LCD, the load level is very large up to 16.33, which means every single pixel unit needs to be responsible for 16.33 light rays in average. Obviously, the single pixel unit fails to give consideration to all 16.33 light rays.

From the analysis above, there are two solutions for the light field decomposition, one is adding controllable units and another one is reducing the load. What follows in this paper will demonstrate that the second strategy provides more effective solution for light field decomposition at a cheaper price.

Considering the first solution, more LCD layers bring more controllable units but at price of reducing brightness and increasing hardware cost. Generally, we assume the LCD has same resolution with light field view image. Only when the layers of LCD equal to the views of light field, the load level can reach to 1 and then the target light field can be displayed perfectly. For example, a regular light field (7*7) requires up to 49 LCD panels to display light field perfectly. However, the transmittance of the off-the-shelf LCD panel is not so satisfied which is generally lower than 10%. The display brightness will be reduced rapidly along with the increasing of LCD layers. We decompose the target light field at resolution of 7x7x384x512 (e.g. Messerschmitt and Dice[22]) based on different LCD layers, as shown in Figure 5. And the visualization of decomposition results based on 3 layers is shown in the Figure 6 and Figure 7. The fidelity of reconstructed light field greatly improve at the beginning of layer's increasement: the reconstruction quality increases quickly from 2 layers to 3 layers, while the fidelity increasing rate slows down when more layers are utilized, because the load level reduces most quickly from 2 layers to 3 layers. Additionally, adding a small number of LCD layer make limited contribution to improve the display quality. Great improvement of display quality requires a large growing of LCD layers. No significant improvement is gained by adding one more LCD layer.

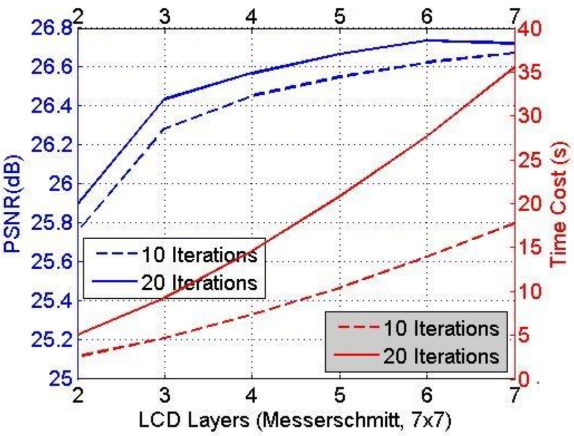

Figure 5. The curve of light field fidelity and time cost along with increasing of the LCD layers

We visualize the decomposition results based on 3 layers in the Figure 6 and Figure 7. As shown in Figure 6 (a) and Figure 7 (a), 3x3 views sub-array extracted from 7x7 target light field and reconstructed light field are compared. The horizontal and vertical parallax is restored successfully. Both the in-focus parts and out-focus parts are reconstructed with high quality. The reconstructed light field inevitably loses fidelity because the LCD layers are much less than the views in target light field. We can see some smear ghost around the outline of the object in the reconstructed light field, such as the fringe of the red dice.

As shown in Figure 6 (b) and Figure 7 (b), the layer images look like three slices in the physical space of the scene: the scene plane near the viewers seems more clear (in focus) in layer 3 image, the scene plane far away the viewers seems more clear in layer 1 image. For example, in the Messerschmitt scene, the sand ground is the nearest part to the viewers, the stern of the car is a little farther to the viewers and the head of the car is farthest part to the viewers. The sand ground is in focus in layer 3 image but the body of the car is out of focus in the layer 3 image. In the layer 2 image, the stern of the car is in focus but the sand ground and the head of the car is blurring. Similarly, the head of the car is clear in layer 1 which is farthest to the viewers. We also found this phenomenon in other scenes, such as dices shown in Figure 7 (b). The green dice which is the farthest part is clear in layer 1 bur blurring in other layers. The red dice is in focus in middle layer. The blue dice is clearest in layer 3.

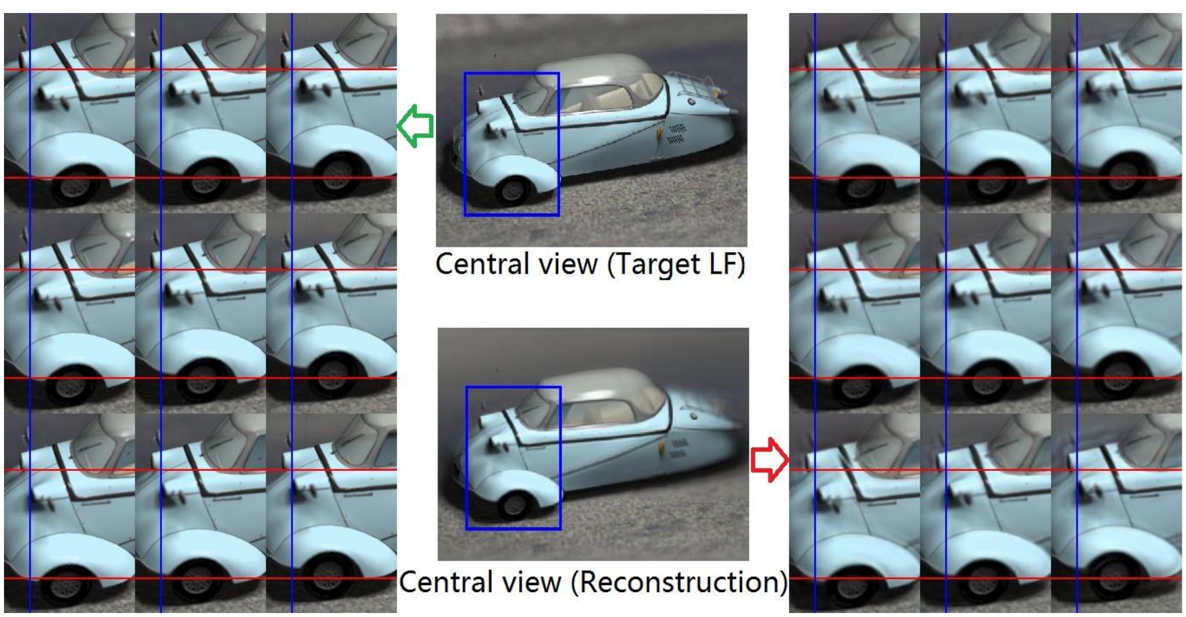

(a) Comparing the target light field with the reconstructed light field

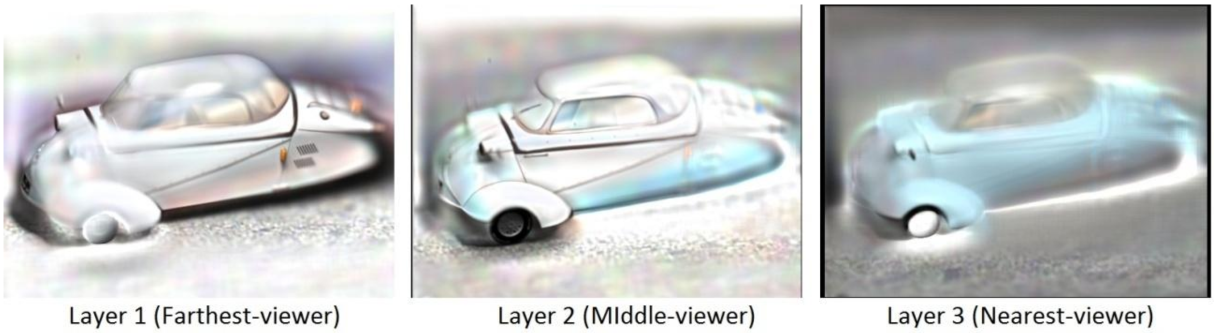

(b) Three layer images decomposed by algorithm in section 4

Figure 6. Visualization of decomposition (Messerschmitt, 7x7)

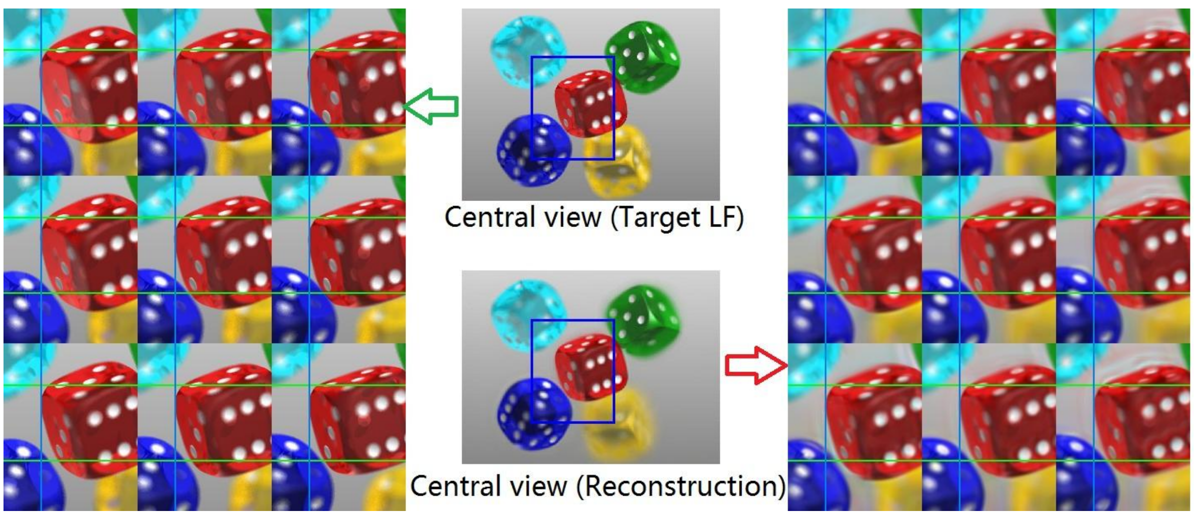

(b) Comparing the target light field with the reconstructed light field

(a) Three layer images decomposed by algorithm in section 4

Figure 7. Visualization of decomposition (Dice, 7x7)

Tensor display[10] represents the light field by summation of multiple frames which increases the degree of freedom, as shown in Figure 8. The amount of controllable units increases over several times by combining multiple frames to display the single light field. However, for single frame decomposition, the load imposed on LCD pixels keeps heavy.

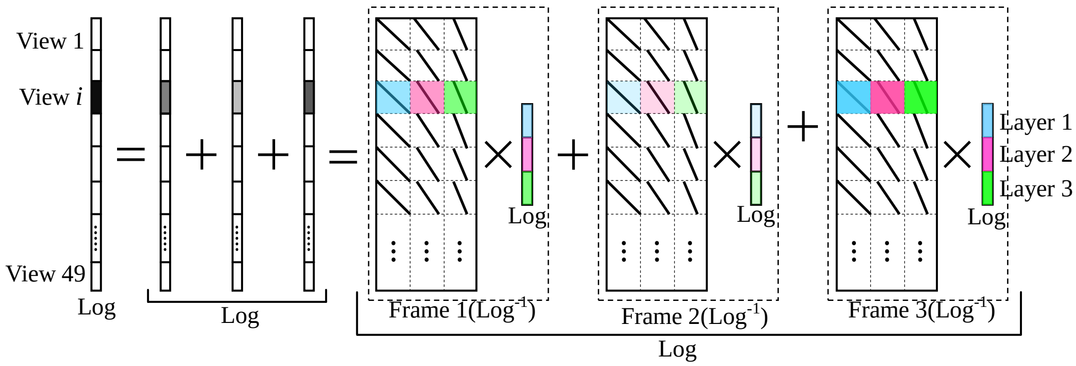

Figure 8. Multi-layer and multi-frame joint optimization strategy

6. LOAD-BALANCING LIGHT FIELD DECOMPOSITION

From the above analysis, additional LCD layers fail to improve display quality significantly. Multi-frames strategy provides more controllable variables, but the load level is still high. In this section, we propose multi-layer and multi-zone joint optimization strategy to lighten load level and improve reconstruction quality significantly. Firstly, the target light field is divided into several subzones, as shown in Figure 9. Each subzone of light field is expressed as Eq. (6).

$$\begin{cases} \mathrm{L} = \{\mathrm{L}_i | \mathrm{i} = 1, 2, \cdots \mathrm{M}\} \\ \mathrm{L}_i = [\mathrm{A}_i, \mathrm{B}_i, \mathrm{C}_i] \end{cases} \tag{6}$$

where L denote the target light field which is divided into M subzones, and L_i is the i -th subzone of L; A_i, B_i and C_i are the three LCD layers for displaying i -th subzone. The refresh rate of LCD panel in our prototype is 144Hz. So we divide light field into 4 subzones in order to make sure the light field can be displayed at least 30Hz preventing apparent flicker.

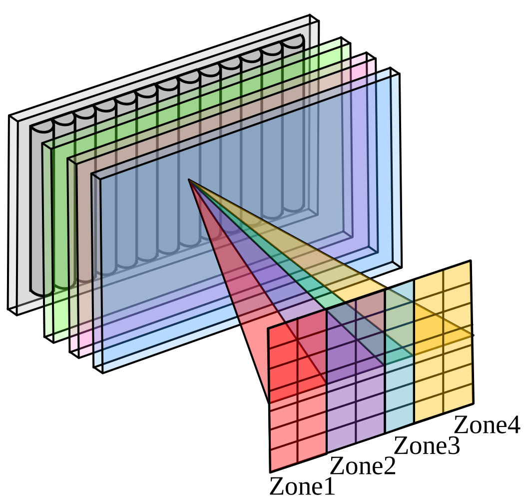

Figure 9. Multi-LCD and multi-zone joint optimization

Comparing to multi-frame decomposition strategy in Figure 8, our multi-layer and multi-zone joint optimization strategy is visualized in Figure 10. Each subzone of target light field is displayed by all LCD layers but the amount of target light rays is reduced significantly. So the average load drops to a much lower level. Both the multi-frame in [Wetzstein et al. 2011][10] and our multi-zone bring multiple times of controllable units. Unlike multi-frame, our multi-zone optimization reduces the load level in single light field decomposition. In other word, multi-frame strategy requires the three LCD layers to be responsible for all 49 views in single frame decomposition; while the three LCD layers only need to be responsible for 14 views in single zone decomposition by our multi-zone decomposition strategy.

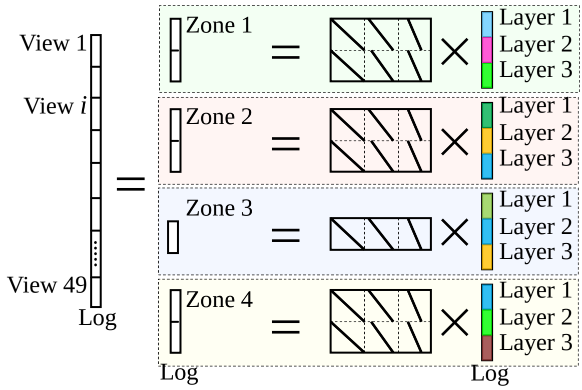

Figure 10. Multi-layer and multi-zone joint optimization strategy

As shown in Figure 11, we decompose subzone light field of different size when LCDs keep constant three layers. The fidelity of reconstructed light field increases significantly along with the decreasing of light field's size. In addition, the computation cost also decrease greatly. Thus, comparing to the strategy of increasing layers shown in Figure 5, our load-balancing solution shown in Figure 10 exhibits more superiority: 1) less LCD layers reduce the loss of light transmission and display light field more brightly; 2) less layers and smaller light field size reduce the computation cost significantly; 3) the quality of reconstruction improves without requiring extra layers; 4) our multi-layer and multi-zone joint optimization utilizes the spatial independence of light field exploring the parallax decomposition among multiple subzones.

We also found the quality and efficiency of light field decomposition depends on the scene. And the required iterations to converge decrease along with the decreasing of light field size. For example, in the decomposition of Messerschmitt shown in Figure 11, the PSNR of 20 iterations is a little less than that of 10 iterations when light field size is less than 7x3. The decomposition algorithm converges after 10 iterations, more iterations may cause oscillation. So it's not necessary to waste more computation source on more iterations in small size light field decomposition. For decomposition of Dice, similar phenomenon appears when light field size is less than 7x2.

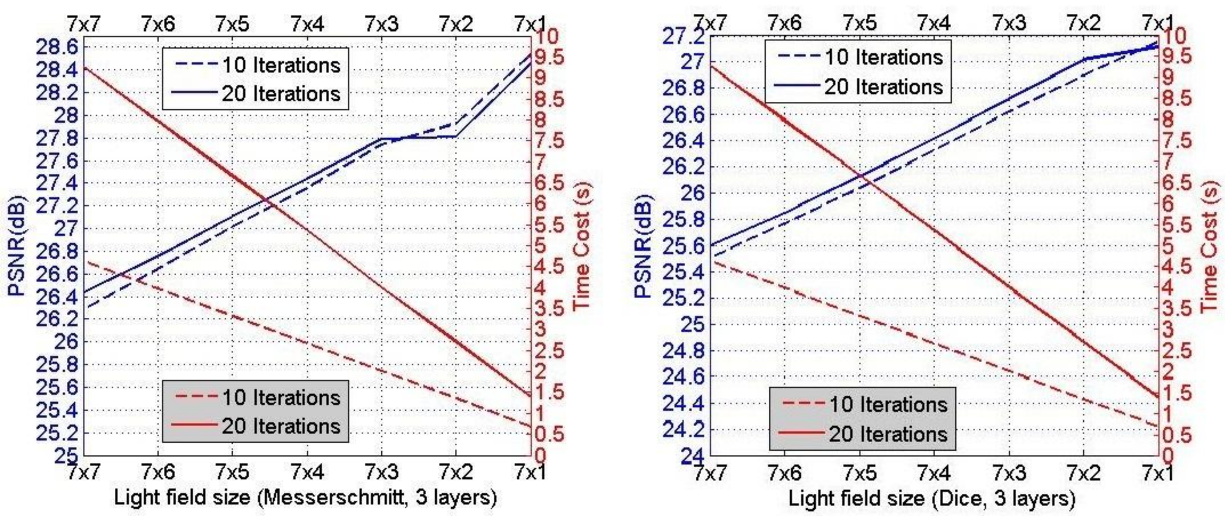

Figure 11. The curve of light field fidelity and time cost along with decreasing of the light field size

7. DYNAMIC DIRECTIONAL BACKLIGHT

The load-balancing light field display presented in this paper requires the backlight source to alternatively provide directional light for different light field subzones which is similar to time-sequential backlight in [Kwon et al.][23] but in different design. LCD covered with lenticular lens sheet provides a good approach to achieve such dynamic directional backlight. But calibration and alignment between LCD and lens sheet is very challenging. The perfect directional light can be produced only if lens cylinder covered integral number of pixels. Minor deviation resulted by misalignment accumulates and degrades the display effect seriously. To our best knowledge, there is no off-the-shelf LCD and lens sheet matched perfectly. Many approaches have been proposed to overcome these drawbacks by slanting the lenticular lens at a small angle[24,25]. Slanted lenticular lens sheet, however, needs complicated process to remap the pixels and has low light transmission. We mount the lenticular lens sheet tightly on the LCD without slanting and make sure that each pixel is in the focal plane of lens. The key design in our dynamic directional backlight is to establish independent coordinate system for each lens cylinder, as shown in Figure 12. The horizontal axis is for pixel shift from the origin. And the vertical axis is for amplitude of pixel bisecting the lens cylinder. The normal direction of lens sheet is defined as zero angle.

$$\alpha = \frac{x}{L} A_{Period}, \quad s.t. -\frac{1}{2} A_{Period} < \alpha < \frac{1}{2} A_{Period}$$

where, α is the angle of expected directional backlight, x is the shift from origin of coordinates; L and A_{Period} denote width of signal lens cylinder and period angle of lens sheet respectively, which can be gained from the lens sheet reference manual.

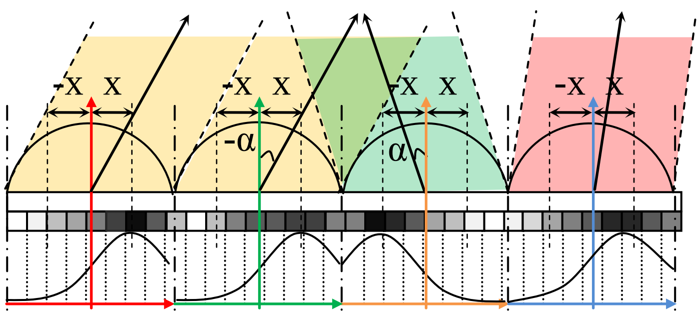

Figure 12. Coordinate system for lens

We construct a backlight control curve to determinate the direction and sharpness of expected directional backlight. The phase angle of control curve is the angle of expected backlight and curve's sharpness determines the sharpness of expected backlight. The pixel values equal to the integration of the curve during the pixel width. Compared to traditional slanted lens sheet, our designs require no alignment between the lens sheet and integral pixels. And the offset resulted by misalignment don't accumulate and expand. Each lens cylinder is controlled independently and can emit backlight in different direction. By combining different direction, we can emit different pattern backlight. For example, a parallel backlight can be achieved by assigning same control curve for every lens cylinder, such as first and second cylinder lens in Figure 12. It can also emit cone-shaped light rays focusing on a spatial point like the second and third cylinder lens in Figure 12. Additionally, the pixels can be lightened in grayscale which is not restricted in zero-one value. And multiple even all pixels are turned on which increases the utilization efficiency of backlight source and display brightness. We also design a LED array backlight source to future increase the display brightness which can support bright light field display in the indoor lighting environment.

8. IMPLEMENTATION

We construct three layers display system, as shown in Figure 15. The model of LCD panel is ASUS VG 278H which has resolution of 1920*1080 and refresh rate up to 144Hz. Polarizing films are interpolated between adjacent two LCD panels and another two polarizing films are mounted outside of the first and last LCD panels. The polarity of these films keeps orthogonal with adjacent films. Due to the upper bound of LCD's refresh rate (144Hz), we divide the target light field into four subzones, as shown in Figure 9, for making sure the display rate can reach to 30Hz.

We decompose a 7x3x540x960 light field (Fish shown in Figure 14). The decomposition performance of four subzones is shown in Table 1. The average of PSNR reaches to 28.8152dB. We take three photos from different viewpoints within the scope of about 10 degrees. Comparing Figure 14 and Figure 15, the parallax is displayed correctly.

Table 1. Performance of four subzones' decomposition based on three layers

	Zone 1 (2x2)	Zone 2 (2x2)	Zone 3 (2x1)	Zone 4 (2x2)	Average
PSNR (dB)	28.7253	28.7118	29.1025	28.7214	28.8152

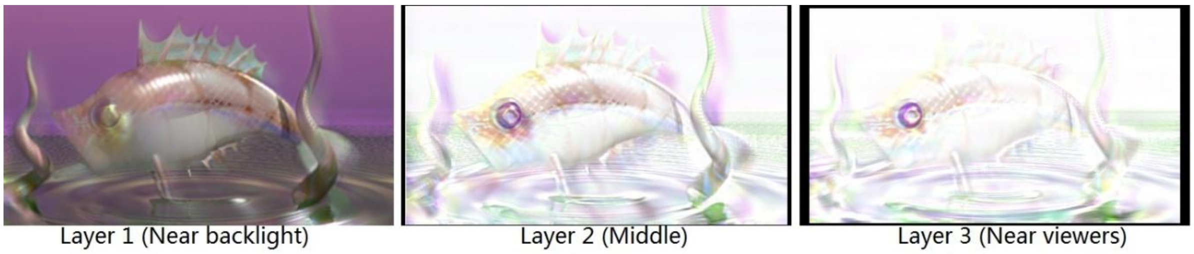

Figure 13. Layer images of decomposition in zone 1

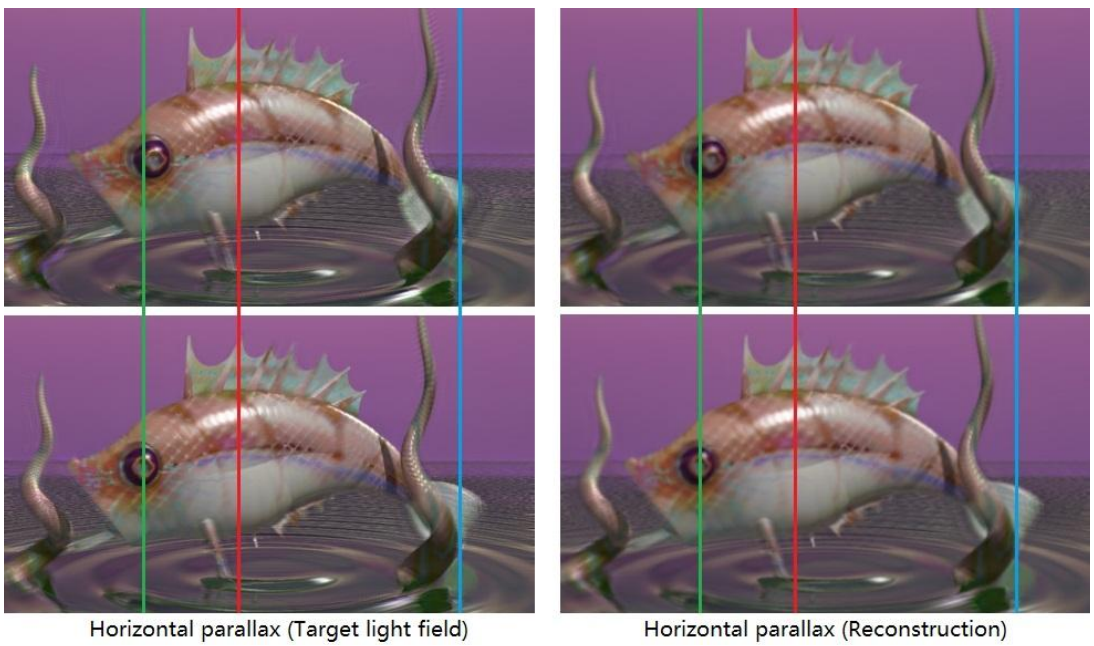

Figure 14. Horizontal parallax between zone 1 and zone 4

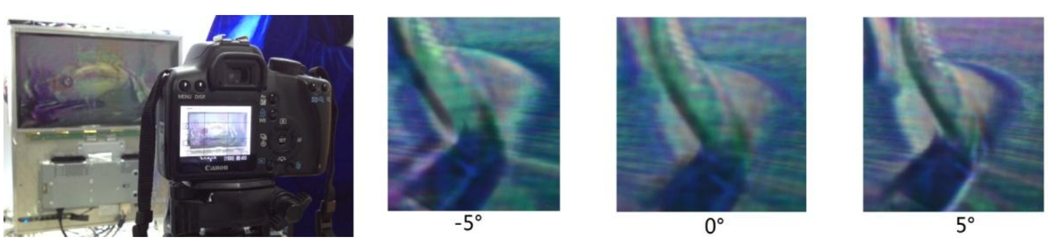

Figure 15. Three layers display prototype in indoor lighting environment

9. FUTURE WORKS

The distance between adjacent LCD panels determines the spatial multiplexing of LCD pixels and the transform matrix. We will do deep research on the parameters optimization and spatial calibration of multi-LCD. The light field decomposition algorithm in section 4 seems to automatically focus in different distance of the scene, which may provide a novel solution to refocus. It remains a promising future direction. The iterative algorithm proposed in this paper explores the spatial independence and parallelity. In the next step, we will utilize multiple GPUs and CUDA technology to implement image-based light field decomposition in real time.

10. CONCLUSION

Multiple LCD provides a novel solution for light field display. We construct a simple and straightforward model to analyze the light field decomposition and found that increasing LCD layers is not an effective way to improve light field fidelity. The load-balancing light field display proposed in this paper resolves the target light field and further explore the capability of light field displaying. We also construct a prototype to demonstrate that our load-balancing light field display based on multiple LCD panels provides correct parallax and occlusion. We hope the technologies discussed in this paper provide insightful schemes for effective and high-quality light field display in the future.

ACKNOWLEDGMENTS

This work has been supported by the National High-tech R&D Program (863 Program) of Institute of Automation, Chinese Academy of Sciences (CASIA), grant 2012AA011903. Special appreciations to the light field data source providers who made this study possible.

REFERENCES

[1] Lipton, L., [Foundations of the Stereoscopic Cinema], Van Nostrand Reinhold Publishers, New York, (1982).

[2] Geng, J., "Three-dimensional display technologies," Adv. Opt. Photonics 5(4), 456–535 (2013).

[3] Jones, A., Mcdowall, I., Yamada, H., Bolas, M., and Debevec, P., "Rendering for an interactive 360 °light field display," ACM Trans. Graph. 26(3), Artn 40 (2007).

[4] Jones, A., Lang, M., Fyffe, G., Yu, X., Busch, J., McDowall, I., Bolas, M., Debevec P., "Achieving Eye Contact in a One-to-Many 3D Video Teleconferencing System," ACM Trans. Graph. 28(3), Artn 64 (2009).

[5] Ng, R., Levoy, M., Bredif, M., Duval, G., Horowitz, M., and Hanrahan, P., "Light field photography with a hand-held plenoptic camera," Tech. rep., Stanford University, (2005).

[6] Venkataraman, K., Lelescu, D., Duparre, J., McMahon, A., Molina, G., Chatterjee, P., Mullis, R., and Nayar, S., "PiCam: An ultra-thin high performance monolithic camera array," ACM Trans. Graph. 32(6), Artn 166 (2013).

[7] Cao X., Geng, Z., and Li, T., "Dictionary-based light field acquisition using sparse camera array," Optics Express, 22(20), 24081-24095 (2014).

[8] Lanman, D., Hirsch, M., Kim, Y., and Raskar, R., "Content-adaptive parallax barriers: optimizing dual-layer 3D displays using low-rank light field factorization," ACM Trans. Graph. 29(6), Artn 163 (2010).

[9] Wetzstein, G., Lanman, D., Heidrich, W., and Raskar, R., "Layered 3D: Tomographic image synthesis for attenuation-based light field and high dynamic range displays," ACM Trans. Graph. 30(4), Artn 95 (2011).

[10] Wetzstein, G., Lanman, D., Hirsch, M., Raskar. R., "Tensor Displays: Compressive Light Field Synthesis using Multilayer Displays with Directional Backlighting" ACM Trans. Graph. 31(4), Artn 80 (2012).

[11] Barnum, P. C., Narasimhan, S. G., and Kanade, T., "A multi-layered display with water drops," ACM Trans. Graph. 29(4), Atrn 76, 1–7 (2010).

[12] Bell, G. P., Craig, R., Paxton, R., Wong, G., and Galbraith, D., "Beyond flat panels: Multi-layered displays with real depth" SID Digest 39(1), 352–355 (2008).

[13] Date, M., Hisaki, T., Takada, H., Suyama, S., and Nakazawa, K., "Luminance addition of a stack of multidomain liquid-crystal displays and capability for depth-fused three-dimensional display application," Applied Optics 44(6), 898–905 (2005).

[14] Gotoda, H., "A multilayer liquid crystal display for autostereoscopic 3D viewing," SPIE Stereoscopic Displays and Applications XXI, 7524, 1–8 (2010).

[15] Kim, Y., Kim, J., Kang, J. M., Jung, J. H., Choi, H., and Lee, B., "Point light source integral imaging with improved resolution and viewing angle by the use of electrically movable pinhole array," Optics Express 15(26), 18253–18267 (2007).

[16] Lanman, D., Wetzstein, G., Hirsch, M., Heidrich, W., Raskar, R., "Polarization Fields: Dynamic Light Field Display using Multi-Layer LCDs," ACM Trans. Graph. 30(6), Artn 186 (2011).

[17] Kolda, T. G., and Bader, B. W., "Tensor decompositions and applications," SIAM Review 51(3), 455–500 (2009).

[18] Blondel, V., Ho, N., and Van Dooren, P., "Weighted nonnegative matrix factorization and face feature extraction," Image and Vision Computing, 1–17 (2008).

[19] Levoy, M., and Hanrahan, P., "Light field rendering," Proc. ACM SIGGRAPH, 31–42 (1996).

[20] Andersen, A., and Kak, A., "Simultaneous Algebraic Reconstruction Technique (SART): A superior implementation of the ART algorithm," Ultrasonic Imaging 6(1), 81–94 (1984).

[21] Keck, B., Hofmann, H., Scherl, H., Kowarschik, M., and Hornegger, J., "GPU-accelerated SART reconstruction using the CUDA programming environment," Proc. SPIE 7258, (2009).

[22] http://web.media.mit.edu/~gordonw/SyntheticLightFields/

[23] Kwon, H., and Choi, H. J., "A time-sequential multiview autostereoscopic display without resolution loss using a multidirectional backlight unit and an LCD panel," SPIE Stereoscopic Displays and Applications XXIII 8288, 1–6 (2012).

[24] Van Berkel, C., "Image Preparation for 3D-LCD," Stereoscopic Displays and Virtual Reality Systems VI 3639, 84-91 (1999).

[25] Van Berkel, C., and Clarke, J. A., "Characterisation and optimisation of 3D-LCD module design," Stereoscopic Displays and Virtual Reality Systems IV 3012, 179-186 (1997).